Analytica Chimica Acta 1009 (2018) 12–19

Contents lists available at ScienceDirect

Analytica Chimica Acta

journal homepage: www.elsevier.com/locate/aca

Direct analysis of aluminum alloys by CSigma laser-induced breakdown spectroscopy

C. Aragón [a, b, *], J.A. Aguilera [a, b]

[a] Departamento de Física, Universidad Pública de Navarra, Campus de Arrosadía, E-31006 Pamplona, Spain
[b] Institute for Advanced Materials (INAMAT), Public University of Navarre, Campus de Arrosadía, E-31006 Pamplona, Spain

HIGHLIGHTS

- Cσ-LIBS has been applied to direct analysis of aluminum alloys.
- After characterization with one sample, six certified alloys are analyzed.
- Average precision of 8.0% is obtained for concentrations higher than 0.1 wt %.

GRAPHICAL ABSTRACT

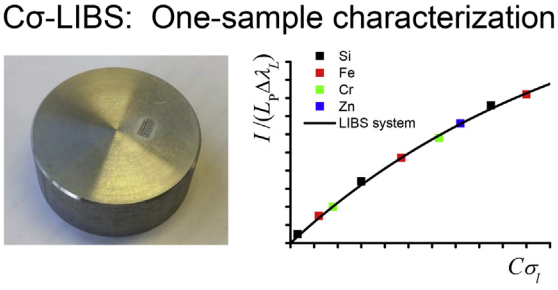

ARTICLE INFO

Article history:
Received 26 October 2017
Received in revised form
10 January 2018
Accepted 12 January 2018
Available online 20 January 2018

Keywords:
Laser-induced breakdown spectroscopy
LIBS
CSigma LIBS
Quantitative analysis
Standardless analysis
Aluminum alloys

ABSTRACT

We report the application of CSigma laser-induced breakdown spectroscopy (Cσ-LIBS) to quantitative analysis of aluminum alloys without sample preparation. Cσ-LIBS simplifies strongly the conventional calibration procedure of LIBS, replacing it with a characterization stage performed from the spectrum of a single standard sample. The aim of this work has been to provide a complete evaluation of the use of Cσ-LIBS for direct analysis by obtaining its figures of merit, including precision and limits of detection. Ten elements (Si, Fe, Cu, Mn, Mg, Cr, Ni, Zn, Ti and Ca) are determined in a set of six certified samples with a wide range of concentrations, from percent down to μg/g levels. The average precision is 8.0% for concentrations higher than 0.1 wt% and 13% for concentrations between 0.1 wt% and 0.01 wt%. The limits of detection are in the range 1.4–9.7 μg/g.

1. Introduction

Among the spectroscopic techniques allowing direct quantitative analysis of samples, laser-induced breakdown spectroscopy (LIBS) has attracted high interest due to its operational simplicity, versatility and relatively low cost [1]. Moreover, the use as spectroscopic source of a laser-induced plasma, which accomplishes local thermodynamic equilibrium (LTE) in many experimental situations, has prompted the formulation of so-called calibration-free laser-induced breakdown spectroscopy (CF-LIBS), proposed in 1999 by Ciucci et al. [2]. The features that make this concept so attractive are that it allows quantitative standardless analysis and its ability to overcome matrix effects. However, several experiments have shown that this method presents important limitations, specially a poor accuracy for minor components [3]. To improve the analytical performance, new approaches have relaxed

* Corresponding author.
E-mail addresses: carlos.aragon@unavarra.es (C. Aragón), j.a.aguilera@unavarra.es (J.A. Aguilera).

https://doi.org/10.1016/j.aca.2018.01.019

the concept of calibration-free by considering the use of one or a few standard samples. Replacing the tedious conventional procedure of calibration for each element using a wide set of standards with a simpler measurement of the spectrum of one standard sample still entails a great simplification of the analytical process. Moreover, a frequent re-calibration of the analytical instrument using this simplified measurement is also an appealing possibility provided by these methods. Gaudiuso et al. [4] proposed so-called inverse CF-LIBS, an approach where the key plasma temperature is determined by minimization of the errors of concentrations determined for one standard sample. The Pisa group presented a variant of their original formulation of the method called one-point-calibration CF-LIBS [5], consisting in the empirical determination from a standard sample spectrum of essential experimental and spectroscopic parameters, whose knowledge is often imprecise or lacking. Our group has proposed recently CSigma laser-induced breakdown spectroscopy (Cσ-LIBS) [6,7], where Cσ graphs are obtained using at least one standard sample, after which the system becomes characterized and other samples may be analyzed. For a spectral line showing self-absorption, curves of growth are graphs of the line intensity vs. the optical depth, the latter being proportional to the elemental concentration in a sample. The curve of growth methodology was applied the first time to LIBS by Gornushkin et al. [8]. Cσ graphs may be considered as generalized curves of growth, as they allow to include several spectral lines of various elements in the same plot. The initial demonstration of Cσ-LIBS for slag analysis was presented in Ref. [6] and a second validation with a set of rock samples having a wider range of concentrations has been performed recently [9]. In both works, certified reference materials in powder form were prepared as fused-glass samples. Although fused-glass samples have been very convenient for the initial testing of Cσ-LIBS, they present some drawbacks, the main one being of course the time required for preparation, which nullifies the characteristic readiness of LIBS analysis. Also, the dilution of the sample increases the limits of detection, and the possibility of contamination by traces present in the solvent or accidentally during the preparation process is always present. Therefore, demonstration of the applicability of Cσ-LIBS to direct analysis, without sample preparation, is a relevant issue at the moment. Quantitative direct analysis by LIBS using the methods based on a plasma in LTE entails significant difficulties, such as the greater self-absorption of spectral lines expected for the higher concentrations in the samples, compared to those present in the diluted fused glass samples, and the higher chance of failure of the simple model used for the laser-induced plasma.

To our knowledge, the only work where Cσ-LIBS has been applied to direct analysis is a recent article by Grifoni et al. [10]. In this work, three methods including one-point-calibration CF-LIBS, inverse CF-LIBS and Cσ-LIBS are tested and compared on spectra acquired on modern bronze samples. The average percent error obtained for Cσ-LIBS for the four elements analyzed is 19%, a relatively high value taking into account that the elemental concentrations in the six samples used exceeded 0.8% in all cases. A study of the limits of detection is not included in this work. Our goal in the present work has been to test Cσ-LIBS for direct analysis, performing a complete check of the analytical figures of merit. To this aim, we have used a wide set of aluminum alloys, including elements with concentrations from percent down to μg/g levels, which has allowed us to determine the precision for different contents and to estimate the limits of detection.

2. Experimental

The LIBS experimental setup was the same used previously [9], so it is only described briefly, highlighting changes performed. Laser-induced plasmas are generated in air at atmospheric pressure by a Nd:YAG laser (wavelength 1064 nm, pulse energy 60 mJ, pulse width 4.5 ns, repetition rate 20 Hz) focused by a lens of 126-mm focal length with a lens-to-sample distance of 116 mm. For collecting the plasma emission, we modified the previous configuration based on image formation with a system of mirrors, replacing it with a 0.22 numerical aperture optical fiber of 600-μm core diameter, placed at 10 mm from the plasma. The use of the optical fiber has allowed to improve the long-term stability of the intensity of the spectra. The fiber transmits the radiation from the plasma to a Czerny-Turner spectrometer (focal length 0.5-m, grating of 3600 lines mm^{-1}), equipped with an intensified charge-coupled device detector. The spectral efficiency of the system has been measured using radiance-calibrated deuterium and tungsten standard lamps. Each spectrum results from the accumulation of 100 laser shots while the sample rotates at 100 rpm. All the spectra were acquired with a time delay of 1.6 μs from the laser pulse and a time integration gate of 0.9 us. We checked that, at this time window, the spectra showed a good line-to-continuum ratio for both neutral atom and ion emission lines.

The samples used in this experiment are seven aluminum alloy certified reference materials (HYDRO Aluminum Rolled Products GmbH, Germany). The manufacturer produces the reference aluminum alloys by means of DC-casting, which is especially suitable for producing homogeneous samples, and checks the homogeneity of the samples by S-OES and XRF. Anyway, as problems associated with sample inhomogeneity have been reported in laser ablation methods [11], all experimental data have been obtained averaging five measurements at different positions of the sample, so that the effect of a possible remaining inhomogeneity is reduced. The certified samples are cylindrical, of 38 mm diameter and 30 mm height and have been used as supplied by the manufacturer, i.e., the plasmas have been generated on the flat surface without performing any finishing or cleaning action. We have included in the study all the main elements of the samples, i.e. those having concentrations higher than 1 wt% (with the exception of the matrix aluminum element), as well as several minor elements with low concentrations down to the μg/g range. Sample 1004, with trace-level content for all elements, has also been included in order to obtain the limits of detection for some elements whose concentrations are too high in the rest of samples. Sample 3003 has been used in the characterization stage of Cσ-LIBS, and then the rest of the samples have been analyzed for validation.

3. Results and discussion

3.1. Selection of spectral lines

The details of the Cσ-LIBS procedure are described in a previous work [6]. Firstly, the method requires a careful selection of the spectral lines used for characterization and analysis. The lines chosen need to have known accurate oscillator strengths and at least an estimation of their Stark widths. A bibliographic search has been performed to get accurate values of the atomic data which have not yet been included in available atomic databases. Table 1 lists the lines used in the present work to construct the Cσ graphs for aluminum alloy samples, showing their atomic data.

The Cσ-LIBS method is based on a set of parameter definitions. The k_t parameter depends on the plasma temperature T and is given by

Table 1
Spectral lines used to construct the $C\sigma$ graphs, with their atomic data and typical $k_t r_i$ and σ_l values. The use of the lines for characterization (C), analysis (A) or trace analysis (T) is also indicated.

	λ (Å)	E_i (eV)	E_k (eV)	g_i	g_k	f[a]	Acc.	w[b] (Å)	Acc.	$k_t r_i^c$ (10^{-20} m^{2}Å)	σ_l^c (10^{-20} m^2)	Use
Cr I	3578.684	0.00	3.46	7	9	3.66E-01	B	0.1	–	7.49	74.9	C, A
	3593.481	0.00	3.45	7	7	2.91E-01	B	0.1	–	6.00	60.0	C, A
Cu I	2824.368	1.39	5.78	6	6	9.30E-03	C+	0.1	–	0.296	2.96	A
	2961.164	1.39	5.57	6	8	6.59E-03	C+	0.136	C	0.230	1.69	C, A
	3273.952	0.00	3.79	2	2	2.21E-01	AA	0.1	–	15.7	157	C, A, T
Fe I	3631.463	0.96	4.37	7	9	0.131	A	0.1	–	0.8723	8.73	C
	3647.843	0.91	4.31	9	11	0.0711	A	0.1	–	0.646	6.46	C
	3727.619	0.96	4.28	7	5	0.0334	A	0.08	M	0.234	2.93	C
	3749.485	0.91	4.22	9	9	0.161	A	0.08	M	1.54	19.3	C
	3763.789	0.99	4.28	5	5	0.116	A	0.08	20	0.570	7.12	C
	3765.539	3.24	6.53	13	15	0.233	B+	0.07	20	0.220	3.14	C
	3767.192	1.01	4.30	3	3	0.136	A	0.08	20	0.392	4.90	C
Ni I	3414.764	0.03	3.66	7	9	1.20E-01	C	0.076	n/a	4.78	62.9	C, A
	3458.460	0.21	3.80	3	5	1.80E-01	C+	0.15	–	2.54	16.9	C, A
	3461.652	0.03	3.61	7	9	6.20E-02	C+	0.076	n/a	2.54	33.4	C, A
	3492.956	0.11	3.66	5	3	1.10E-01	C+	0.15	–	2.97	19.8	C, A
	3524.536	0.03	3.54	7	5	1.30E-01	C	0.15	–	5.51	36.7	C, A
Si I	2506.897	0.01	4.95	3	5	0.0859	B	0.141	29	4.23	30.0	C, A, T
	2514.316	0.00	4.93	1	3	0.21	B	0.112	29	3.51	31.3	C, A
	2516.112	0.03	4.95	5	5	0.159	B	0.117	31	12.9	110	A, T
	2519.202	0.01	4.93	3	3	0.0522	B	0.112	31	2.60	23.2	C, A
	2524.108	0.01	4.92	3	1	0.0708	B	0.104	33	3.54	34.0	A, T
	2528.508	0.03	4.93	5	3	0.052	B	0.107	35	4.25	39.7	A, T
Zn I	3282.330	4.01	7.78	3	7	0.339	–	0.8	–	3.21	4.01	C, A
	3302.580[d]	4.03	7.78	14	18	0.21	–	0.8	–	9.12	11.4	C, A
	3345.020[e]	4.08	7.78	33	33	0.154	–	0.8	–	15.3	19.1	C, A
Ca II	3933.663	0.00	3.15	2	4	6.82E-01	C	0.17	15	492	2890	C, A
	3968.469	0.00	3.12	2	2	3.30E-01	C	0.16	15	242	1510	A
Fe II	2585.876	0.00	4.79	10	8	0.0717	B+	0.0411	15	5.37	131	C, A
	2591.543	1.04	5.82	6	6	0.0576	B	0.047	15	0.777	16.5	C, A
	2598.370	0.05	4.82	8	6	0.108	B+	0.0395	M	6.18	157	C, A, T
	2599.396	0.00	4.77	10	10	0.239	B+	0.045	15	18.1	402	C, A, T
	2607.088	0.08	4.84	6	4	0.117	B	0.0394	14	4.85	123	C, A, T
	2611.874	0.05	4.79	8	8	0.122	B+	0.0368	14	7.06	192	C, A, T
	2613.825	0.11	4.85	4	2	0.109	B+	0.0384	14	2.95	76.7	C, A, T
	2617.618	0.08	4.82	6	6	0.0501	B	0.038	15	2.10	55.1	C, A
	2621.670	0.12	4.85	2	2	0.0577	B+	0.038	15	0.772	20.3	C, A
Mg II	2790.777	4.42	8.86	2	4	9.37E-01	A	0.162	B+	3.32	20.5	C, A
	2795.528	0.00	4.43	2	4	6.08E-01	A+	0.087	B+	366	4210	T
	2797.998[f]	4.43	8.86	8	10	4.69E-01	A	0.144	B+	6.60	45.8	T
	2802.705	0.00	4.42	2	2	3.03E-01	A+	0.0945	B+	183	1940	T
	2936.510	4.43	8.65	4	2	1.49E-01	A	0.3	B+	1.15	3.84	C, A
Mn II	2593.724	0.00	4.78	7	7	0.279	2.9	0.14	16	71.3	509	A, T
	2605.684	0.00	4.76	7	5	0.196	3.0	0.148	16	50.9	344	A, T
	2933.055	1.17	5.40	5	3	0.158	2.9	0.163	16	9.24	56.7	C, A
	2939.308	1.17	5.39	5	5	0.257	3.0	0.122	16	15.1	124	C, A, T
	2949.205	1.17	5.38	5	7	0.358	3.1	0.16	16	21.3	133	C, A, T
Ti II	3340.341	0.11	3.82	4	4	7.16E-02	B+	0.1	–	2.75	27.5	C, A
	3341.875	0.57	4.28	6	8	3.75E-01	B+	0.1	–	12.6	126	C, A
	3361.212	0.03	3.72	8	10	3.35E-01	C	0.1	–	28.7	287	C, A
	3372.793	0.01	3.69	6	8	3.21E-01	B+	0.1	–	21.2	212	C, A
	3383.758	0.00	3.66	4	6	3.58E-01	B+	0.1	–	16.0	160	C, A
	3394.572	0.01	3.66	6	6	4.65E-02	B+	0.1	–	3.10	31.0	C, A
Zn II	2025.483	0.00	6.12	2	4	0.467	20	0.0537	13	105	1963	T
	2062.004	0.00	6.01	2	2	0.249	20	0.0462	13	58.3	1260	T

[a]Data from Refs. [12] (Cr I, Ni I, Zn I, Ca II, Ti II) [13], (Fe I, Fe II) [14], (Si I) [15], (Mn II) [16], (Zn II).
[b]Stark widths at electron density $N_e = 10^{17}$ cm^{-3} from Refs. [17] (Cu I) [18], (Fe I) [19], (Ni I) [20], (Si I) [21], (Ca II) [22–24], (Fe II) [25,26], (Mg II) [27], (Mn II) [28] (Zn II). When an uncertainty M is displayed in the table, the experimental Stark width is not available, and the average of known Stark widths for lines of the same multiplet has been used. If the uncertainty is not provided, the data come from a rough measurement performed in our laboratory.
[c]Calculated for $T = 10000$ K and $N_e = 10^{17}$ cm^{-3}.
[d]The Zn I lines at 3282.330 Å and 3303.580 Å have been grouped, and the resulting data are indicated.
[e]The Zn I lines at 3345.020 Å, 3345.570 Å and 3345.940 Å have been grouped, and the resulting data are indicated.
[f]The Mg II lines at 2797.930 Å and 2797.998 Å have been grouped, and the resulting data are indicated.

$$k_t = \frac{e^2 \lambda_0^2}{4\varepsilon_0 m c^2} f \frac{g_i e^{-\frac{E_i}{kT}}}{U_\alpha^z(T)} \left(1 - e^{-\frac{E_k - E_i}{kT}}\right), \quad (1)$$

where $U_\alpha^z(T)$ is the partition function for element α in ionization state z of the emitting species, e is the elementary charge, λ_0 is the central wavelength of the transition, ε_0 is the permittivity of free space, m is the electron mass, c is the speed of light in vacuum, k is Boltzmann's constant, f is the transition oscillator strength, g_i is the degeneracy of the lower energy level and E_i, E_k are the energies of the lower and upper energy levels respectively. For a given element,

k_t is proportional to the intensity of the line in the optically thin limit, normalized to the Planck radiance. To account for the different ionization of each element in the plasma, k_t is multiplied by the ionization factor

$$r_i = \frac{1}{1+S^{10}} \qquad \text{for neutral atoms,} \tag{2a}$$

$$r_i = \frac{S^{10}}{1+S^{10}} \qquad \text{for singly-charged ions} \tag{2b}$$

where S^{10} is the ratio between the density of singly-charged ions N_α^1 and that of neutral atoms N_α^0, which depends on temperature T and electron density N_e and is given by

$$S^{10} = \frac{N_\alpha^1}{N_\alpha^0} = \frac{2U_\alpha^1}{N_e U_\alpha^0}\left(\frac{mkT}{2\pi\hbar^2}\right)^{3/2} \exp\left(-\frac{E_\infty^0 - \Delta E_\infty^0}{kT}\right) \tag{3}$$

where h is Planck's constant ($\hbar = h/2\pi$), E_∞^0 is the ionization energy and ΔE_∞^0 is the correction thereof due to interactions in the plasma. Finally, the key parameter of the method is the line cross section σ_l, defined as

$$\sigma_l = k_t r_i \frac{1}{\Delta\lambda_L}, \tag{4}$$

where $\Delta\lambda_L$ is the Lorentzian width that, under the assumption of Stark-broadened profiles, is calculated as the product of the Stark with of the line times the electron density.

To summarize, the product $k_t r_i$ is related to the intensity of the line in the optically thin limit, including the ionization factor, whereas σ_l has to do with its self-absorption [6]. These two parameters are listed in Table 1, calculated for typical values of temperature and electron density. The last column of the table identifies the use of each spectral line for characterization (C), analysis (A) or trace analysis (T). The distinction between lines for characterization and analysis is due to the fact that, for iron, correct Cσ graphs may be constructed from both neutral atom and ion lines. In this case, the Fe II lines have been preferred for analysis due to the higher accuracy resulting from a better signal-to-background ratio. Nevertheless, the Fe I lines contribute to improve the neutral atom Cσ graph, so they have been included for characterization purposes.

A difficulty in the use of laser-induced plasmas for elemental analysis is due to the intrinsic inhomogeneity of these sources, which causes that the emission collected integrates regions having gradients of the fundamental parameters, such as temperature, atomic number densities and electron density. In previous works [29], we have shown that, as a consequence of inhomogeneity, the parameters resulting from characterization by LTE equations are apparent parameters, representing population averages of the true local parameters. Specifically, the apparent temperatures for neutral atoms and ions are different, since the two ionization states occupy different regions of the plasma. This is the reason for using two Cσ graphs and sets of parameters, one for the neutral atom emission and another for the ion emission, which is expressed by the concept of double homogeneous model [6]. In addition, to reduce the effect of the remaining inhomogeneity for each ionization state, a unique feature of Cσ-LIBS is the use of a model limit, allowing to discard from Cσ graphs those data for intense lines and/or high concentrations, for which the double homogeneous model of the plasma fails. To implement the model limit, we have developed an automatic iterated procedure for discarding data exceeding the limit, based on the parameter $\tau_l \Delta\lambda_L$ [6], defined as

$$\tau_l \Delta\lambda_L = \eta Nl\, C\, k_t r_i \tag{5}$$

where Nl is the columnar density, C is the elemental concentrations in units mol g^{-1} and η is a factor for concentration unit conversion. From the experimental Cσ graphs, we have found that the limit of $\tau_l \Delta\lambda_L$ varies depending on the ionization state and Stark width. For

Table 2
Elemental concentration of the 3003 reference sample.

	wt.%	Uncertainty. (wt.%)
Si	7.77	0.13
Fe	0.339	0.009
Cu	0.1420	0.0026
Mn	0.241	0.006
Mg	0.250	0.008
Cr	0.00211	0.00013
Ni	0.0504	0.0012
Zn	0.1182	0.0021
Ti	0.0375	0.0008
Ca	0.00185	0.00007

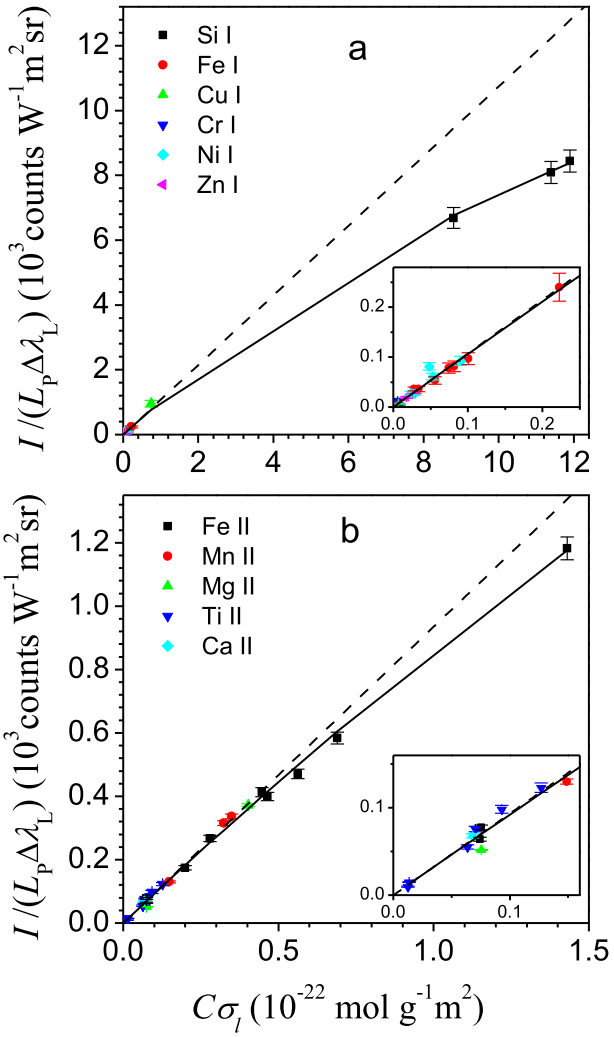

Fig. 1. Characterization Cσ graphs for neutral atom (a) and ion (b) emission lines, obtained with the 3003 certified aluminum alloy. The error bars represent the standard deviation of the average of five measurements at different positions of each sample. The solid line is the fitting providing the plasma parameters. The linear limit of the fittings is shown as a dashed line.

example, the limit is clearly higher for the most intense Mn II line at 2593.724 Å, whose Stark width is around 0.14 Å, compared to that obtained for the most intense Fe II line at 2599.396 Å, which has a lower Stark width of 0.045 Å. The final values of the model limit $(\tau_l \Delta\lambda_L)_{\mathrm{lim}}$ applied here are in the range 0.8–1.2 Å for Si I lines, 0.03–0.05 Å for Fe II lines and 0.07–0.085 for Mn II lines. For sample 1004, the spectral line set (T) is chosen separately, as the trace-level concentrations require and allow to use the most intense resonance lines, which lead to data within the model limit when Cσ graphs are constructed.

The procedure to select the spectral lines for a given sample type starts considering a line set as wide as possible for each element to be determined. A single line is in principle enough to determine the concentration of an element, but the use of a higher number improves the results, as the statistical error and the errors due to the uncertainties of the oscillator strength and Stark width are reduced. Also, a wide set of lines of all elements is required for characterization. Then, some lines are discarded according to the following criteria: (1) lines showing spectral interferences are removed; (2) lines too weak to be measured accurately are discarded; (3) for each sample and element, too intense lines exceeding the model limit are eliminated, as described in the previous paragraph. In case that a given element may be determined from both neutral atom and ion lines, the latter are usually preferred since they normally show higher overall line-to-background ratio.

3.2. Characterization: Cσ graphs for neutral atoms and ions

The characterization stage of Cσ-LIBS is performed using at least one standard sample. Normally, as in the case of the aluminum alloys, only one standard is enough for characterization. The use of several samples is necessary when an element relevant in the material analyzed emits only few lines within the spectral range of the system. In this case, the wider range of concentrations of this element provided by the sample set adds more data to the Cσ graphs, improving the accuracy of the characteristic parameters determined. Also, it may be desirable to use different samples to characterize neutrals and ions. For example, in our previous application of the method to rocks prepared as fused glass samples [9], we used two home-made standards, tailored for characterization of neutral atom and ion emissions. In the present work,

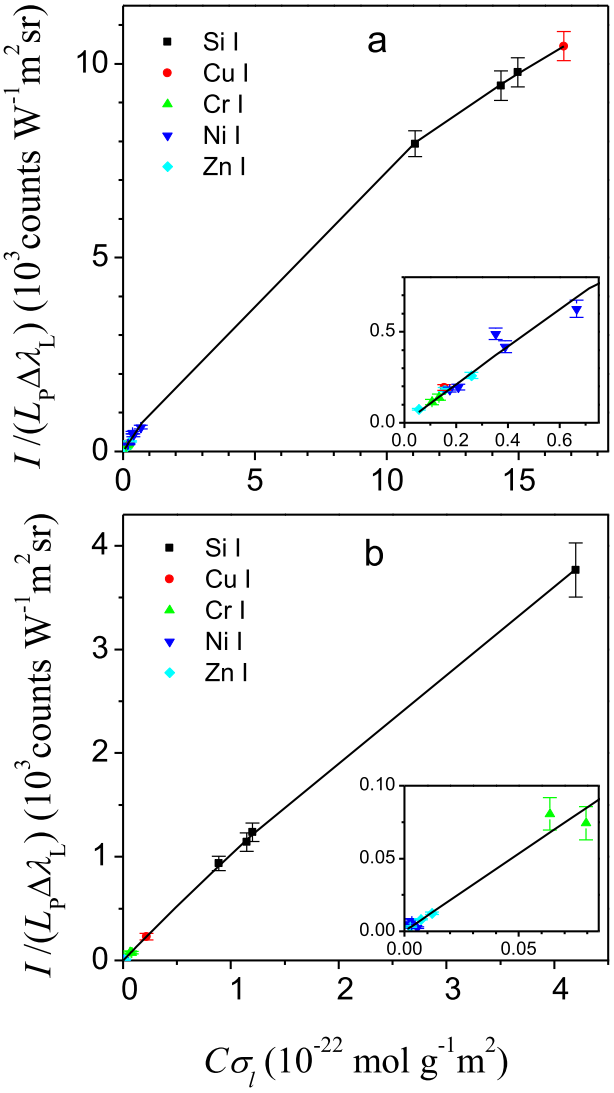

Fig. 2. Final Cσ graphs for neutral atoms resulting from the fitting that provides the Si, Cu, Cr, Ni and Zn concentrations of samples 3053 (a) and 1408 (b). The error bars represent the standard deviation of the average of five measurements at different positions of each sample.

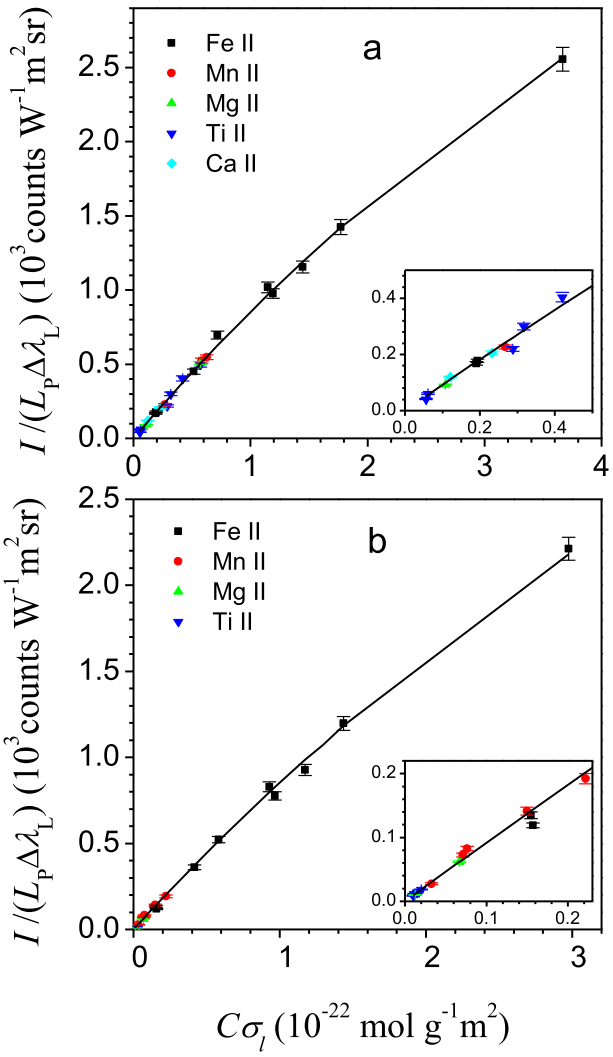

Fig. 3. Final Cσ graphs for ions resulting from the fitting that provides the Fe, Mn, Mg, Ti and Ca concentrations of samples 3053 (a) and 1408 (b). The error bars represent the standard deviation of the average of five measurements at different positions of each sample.

characterization of the laser-induced plasmas has been performed from the spectrum obtained from sample 3003, whose composition is given in Table 2.

In Cσ-LIBS, four parameters (βA, ηNl, T, N_e) characterize each ionization state, allowing to obtain the corresponding Cσ graph by numerical calculation of the expression

$$I = \beta A L_P \int_{\text{line}} \left(1 - e^{-\tau(\lambda)}\right) d\lambda, \tag{12}$$

where A is the transverse area of the region of the of plasma whose emission is detected, β is the instrumental factor of the system and $L_P = L_P(\lambda_0, T)$ is the Planck radiance of a blackbody.

As Cσ graphs data values depend only weakly on the Stark width, in the case of the electron density, a single value $N_e = (1.55\pm0.15) \times 10^{17}$ cm^{-3}, determined from the Stark broadening of the H_α line, is considered for both ionization states [30]. The rest of parameters are obtained from the fitting of the experimental Cσ graphs, shown in Fig. 1. The figure also shows the fitting curves as solid lines, and the linear limits as dashed lines. As can be seen, in the Cσ graph for neutral atoms, the ordinates of the Si I data are well below the linear limit, which means that the lines suffer a significant self-absorption, caused by the high Si concentration in the aluminum 3003 sample. This is in contrast with the low self-absorption of all data found in our previous works [6,9], where Cσ-LIBS was applied to fused glass samples, and represents a major challenge for the method when applied to the direct analysis of samples. The parameters resulting from the fittings are $T^0 = 9100\pm200$ K, $(\eta Nl)^0 = (29\pm7) \times 10^{20}$ g mol^{-1} m^{-2} for neutrals and $T^1 = 12600\pm110$ K, $(\eta Nl)^1 = (60\pm14) \times 10^{20}$ g mol^{-1} m^{-2} for ions. The βA values are not provided, as they depend on the particular instrumental factor of our system.

3.3. Analysis. Results

Once the characteristic parameters are known, the analytical stage starts constructing Cσ graphs for initial arbitrary concentrations. The convergence of a fitting procedure provides the final concentrations and the corresponding Cσ graphs. Fig. 2 shows the final Cσ graphs for neutral atoms, from which the Si, Cu, Cr, Ni and Zn concentrations of samples 3053 (Fig. 2a) and 1408 (Fig. 2b) are obtained. By comparing these plots, we notice the large difference in the content of Si, Cu, Ni and Zn between these samples. Fig. 3a and b shows the Cσ graphs leading to Fe, Mn, Mg, Ti and Ca concentrations in the same samples.

The analytical results for the six aluminum alloys analyzed are shown in Table 3, compared with the certified values. As mentioned in the experimental section, the quoted results correspond to the average of five repeated measurements at different positions of each sample. The uncertainties for the certified element concentrations are shown in the table. To evaluate the accuracy of the method, the relative difference between Cσ-LIBS and certified concentrations is also provided. The average relative difference is 6.9% for concentrations higher than 0.1 wt%, 12.4% for concentrations between 0.1 wt% and 0.01 wt%, and 20.6% for concentrations lower than 0.01 wt%. As mentioned before, these results have been obtained using sample 3003 for characterization. However, any other sample, such as 3002, 3044 or 3053, having elemental concentrations in the range 0.1–10% for several elements, may be used for characterization. To check how the accuracy depends on the characterization sample, we have performed characterization using sample 3053, which has the most different composition from that of sample 3003 within the group of high-content samples, and analyzed the others. The resulting accuracy is slightly worse, the average relative difference with respect to certification being 9.2% for concentrations higher than 0.1 wt%, 13.8% for concentrations between 0.1 wt% and 0.01 wt%, and 21.5% for concentrations lower than 0.01 wt%. The final accuracies reported for the experiment are the averages of the values obtained with both characterization samples, namely, 8.0% for concentrations higher than 0.1 wt%, 13% for concentrations between 0.1 wt% and 0.01 wt%, and 21% for concentrations lower than 0.01 wt%. It is worth stressing the accurate results obtained for Si, in spite of the difficulties due to its high concentration in the aluminum alloys. The comparison of our

Table 3
Concentrations of aluminum samples determined by Cσ-LIBS compared to certified concentrations.

Element	*Cσ*-LIBS (wt.%)	Certified (wt.%)	Unc.[a] (wt.%)	Diff.[b] (%)	*Cσ*-LIBS (wt.%)	Certified (wt.%)	Unc.[a] (wt.%)	Diff.[b] (%)	*Cσ*-LIBS (wt.%)	Certified (wt.%)	Unc.[a] (wt.%)	Diff.[b] (%)
	3002				**5052**				**3044**			
Si	5.85	6.01	0.12	2.6	0.0958	0.090	n/a	6.4	6.49	6.95	0.17	6.6
Fe	0.299	0.310	0.008	3.5	0.19	0.19	n/a	2.2	0.706	0.79	0.07	10.6
Cu	0.303	0.261	0.014	16.2	0.0902	0.059	n/a	52.9	2.51	2.71	0.10	7.4
Mn	0.292	0.281	0.005	3.8	0.27	0.26	n/a	2.4	0.518	0.54	0.07	4.1
Mg	0.184	0.197	0.005	6.4	1.45	1.40	n/a	3.9	0.586	0.675	0.021	13.1
Cr	0.00352	0.00460	0.00011	23.4	0.15	0.15	n/a	2.8	0.00387	0.0044	0.0008	12.2
Ni	0.0787	0.0805	0.002	2.2	–	–		–	0.376	0.372	0.016	1.2
Zn	0.139	0.152	0.004	8.7	2.96	2.99	n/a	0.9	0.431	0.485	0.014	11.1
Ti	0.0663	0.0572	0.0012	15.9	0.0459	0.042	n/a	9.3	0.183	0.164	0.010	11.6
Ca	0.00381	0.00359	0.00019	6.1	–	–	n/a	–	0.0142	0.0129	0.0007	10.0
	3053				**1408**				**1004**			
Si	9.78	10.18	0.17	4.0	0.78	0.82	n/a.	4.5	0.0071	0.0076	n/a	6.0
Fe	0.870	0.985	0.016	11.7	0.71	0.75	n/a	5.9	0.0061	0.0064	n/a	4.8
Cu	3.20	3.65	0.04	12.4	0.0414	0.0346	n/a	19.6	0.0051	0.0036	n/a	41.9
Mn	0.433	0.435	0.010	0.4	0.0526	0.056	n/a	6.1	0.0011	0.0012	n/a	10.6
Mg	0.356	0.402	0.012	11.5	0.0415	0.048	n/a	13.6	0.0031	0.0025	n/a	22.3
Cr	0.0378	0.0379	0.0010	0.3	0.0225	0.0255	n/a	11.7	–	0.00014	n/a	–
Ni	0.371	0.315	0.004	17.8	0.0031	0.0022	n/a	42.4	–	0.00014	n/a	–
Zn	1.046	1.106	0.015	5.4	0.0486	0.048	n/a	1.3	0.0039	0.0068	n/a	43.4
Ti	0.169	0.156	0.004	8.4	0.0060	0.0049	n/a	21.6	–	0.00008	n/a	–
Ca	0.0063	0.0056	0.0006	12.5	–	–	n/a	–	–	0.00007	n/a	–

[a] Uncertainty of certified values if available.
[b] Relative difference between *Cσ*-LIBS and certified concentration.

Table 4
Limits of detection.

Element	C_L (μg/g)
Si	5.8
Fe	5.2
Cu	7.8
Mn	1.8
Mg	1.4
Cr	9.7
Ni	5.3
Zn	4.6
Ti	4.3
Ca	1.4

Cσ-LIBS results with other calibration strategies for LIBS applied to aluminum alloys may be performed for a few references in which the accuracy obtained is provided. Zivkovic et al. [31] have recently investigated the elemental analysis of aluminum alloys by LIBS using a TEA CO_2 laser and conventional calibration curves. They have obtained accuracies between 6 and 13% for element contents higher than 0.01%, which are comparable to our results. Herrera et al. [32] reported a comparative study of CF-LIBS and Monte Carlo simulation in LIBS applied to aluminum alloys under vacuum conditions, obtaining a satisfactory accuracy of 4% for the matrix element Al using the CF-LIBS approach, but only semi-quantitative relative concentrations (30–250% relative errors) for the remainder of the sample components using both approaches.

To estimate the limits of detection, the quantity $(C\sigma)_L = 3s/b$ is firstly calculated from the Cσ graph, where s is the standard deviation of the ordinate for the five repeated measurements performed at different positions of one sample, obtained for data with low concentration, and b is the slope of the linear limit. Then, the limit of detection is obtained as $C_L = (C\sigma_L)/\sigma_L$. Table 4 shows the resulting limits of detection, which are in the range 1.4–9.7 μg/g.

4. Conclusions

Cσ-LIBS may be applied to direct quantitative analysis of aluminum alloys, providing an average accuracy in the range 8.0–21% for concentrations from percent to μg/g levels and limits of detection in the range 1.4–9.7 μg/g. The Cσ-LIBS approach simplifies the conventional LIBS analytical process by replacing calibration for each element using a wide set of standards with a single characterization performed with one sample. Accurate characterization of the laser-induced plasma by means of Cσ graphs has been possible in spite of the high concentrations of some elements, such as Si (up to 10.2 wt%) and Cu (up to 3.65 wt%) in the aluminum samples. Key steps in the application of Cσ-LIBS to direct analysis are a careful selection of spectral lines with known atomic data and a procedure to discard data for intense lines and/or high concentrations, which are described wrongly by the double homogeneous plasma model. As we attribute a significant part of the remaining analytical inaccuracy to the plasma inhomogeneity, future work will include the use of a more complex model of the laser-induced plasma, which reflects the spatial distribution of the parameters.

Acknowledgements

This work has been supported by the project FIS2014-54285-P of the Spanish Ministerio de Economía y Competitividad.

References

[1] J.D. Winefordner, I.B. Gornushkin, T. Correll, E. Gibb, B.W. Smith, N. Omenetto, Comparing several atomic spectrometric methods to the super stars: special emphasis on laser induced breakdown spectroscopy, LIBS, a future super star, J. Anal. At. Spectrom. 19 (2004) 1061–1083.
[2] A. Ciucci, M. Corsi, V. Palleschi, S. Rastelli, A. Salvetti, E. Tognoni, New procedure for quantitative elemental analysis by laser-induced plasma spectroscopy, Appl. Spectrosc. 53 (1999) 960–964.
[3] E. Tognoni, G. Cristoforetti, S. Legnaioli, V. Palleschi, Calibration-free laser-induced breakdown spectroscopy: state of the art, Spectrochim. Acta, Part B 65 (2010) 1–14.
[4] R. Gaudiuso, M. DelÍAglio, O. De Pascale, S. Loperfido, A. Mangone, A. De Giacomo, Laser-induced breakdown spectroscopy of archaeological findings with calibration-free inverse method: comparison with classical laser-induced breakdown spectroscopy and conventional techniques, Anal. Chim. Acta 813 (2014) 15–24.
[5] G.H. Cavalcanti, D.C. Teixeira, S. Legnaioli, G. Lorenzetti, L. Pardini, V. Palleschi, One-point calibration for calibration-free laser-induced breakdown spectroscopy quantitative analysis, Spectrochim. Acta, Part B 87 (2013) 51–56.
[6] C. Aragón, J.A. Aguilera, Quantitative analysis by laser-induced breakdown spectroscopy based on generalized curves of growth, Spectrochim. Acta, Part B 110 (2015) 124–133.
[7] J.A. Aguilera, C. Aragón, Public University of Navarre, WO2015–104049; US Pat. 15110476, 2016; European Pat. 14700162.2, 2016.
[8] I.B. Gornushkin, J.M. Anzano, L.A. King, B.W. Smith, N. Omenetto, J.D. Winefordner, Curve of growth methodology applied to laser-induced plasma emission spectroscopy, Spectrochim. Acta, Part B 54 (1999) 491–503.
[9] J.A. Aguilera, C. Aragón, Analysis of rocks by CSigma laser-induced breakdown spectroscopy with fused glass sample preparation, J. Anal. At. Spectrom. 32 (2017) 144–152.
[10] E. Grifoni, S. Legnaioli, G. Lorenzetti, S. Pagnotta, F. Poggialini, V. Palleschi, From Calibration-Free to Fundamental Parameters Analysis: a comparison of three recently proposed approaches, Spectrochim. Acta, Part B 124 (2016) 40–46.
[11] X.R. Liu, G. Horlick, In situ laser ablation sampling for inductively coupled plasma atomic emission spectroscopy, Spectrochim. Acta 50B (1994) 537–548.
[12] A. Kramida, Ralchenko Yu, J. Reader, NIST ASD Team, NIST Atomic Spectra Database (version 5.5.2), 2018 [Online]. Available, http://physics.nist.gov/asd.
[13] J.R. Fuhr, W.L. Wiese, A critical compilation of atomic transition probabilities for neutral and singly ionized iron, J. Phys. Chem. Ref. Data 35 (2006) 1669–1809.
[14] D.E. Kelleher, L.I. Podobedova, Atomic transition probabilities of silicon. A critical compilation, J. Phys. Chem. Ref. Data 37 (2008) 1285–1501.
[15] E.A. Den Hartog, J.E. Lawler, J.S. Sobeck, C. Sneden, J.J. Cowan, Improved log(gf) values of selected lines in Mn I and Mn II for abundance determinations in FGK dwarfs and giants, Astrophys. J. Suppl. 194 (2011) 35 (11pp).
[16] R. Mayo, M. Ortiz, J. Campos, Experimental oscillator strengths of Zn II lines of astrophysical interest, Eur. Phys. J. D 37 (2006) 181–186.
[17] M. Skočić, M. Burger, Z. Nikolić, S. Bukvić, S. Djeniže, Stark broadening in the laser-induced Cu I and Cu II spectra, J. Phys. B: At. Mol. Opt. Phys. 46 (2013), 185701 (6pp).
[18] J.A. Aguilera, C. Aragón, Spectrochim. Acta Part B, 2008, Characterization of laser-induced plasmas by emission spectroscopy with curve-of-growth measurements. Part I: temporal evolution of plasma parameters and self-absorption, Spectrochim. Acta, Part B 63 (2008) 784–792.
[19] S. Djeniže, Lj. Skuljan, J. Labat, S. Bukvić, R. Konjević, Measured Stark widths and shifts of several NiI and NiII spectral lines, Astron. AstroPhys. Suppl. 105 (1994) 115–118.
[20] S. Bukvić, S. Djeniže, A. Srećković, Line broadening in the Si I, Si II, Si III, and Si IV spectra in helium plasma, Astron. & Astrophys 508 (2009) 491–500.
[21] J.A. Aguilera, C. Aragón, J. Manrique, Measurement of Stark widths and shifts of Ca II spectral lines, Mon. Not. Roy. Astron. Soc. 444 (2014) 1854–1858.
[22] C. Aragón, P. Vega, J.A. Aguilera, Stark width measurements of Fe II lines with wavelengths in the range 260-300 nm, J. Phys. B: At. Mol. Opt. Phys. 44 (2011), 055002 (7pp).
[23] J.A. Aguilera, J. Manrique, C. Aragón, Stark width measurements of FeII lines with wavelengths in the range 230–260 nm, J. Phys. B: At. Mol. Opt. Phys. 44 (2011), 245701 (6pp).
[24] C. Aragón, J.A. Aguilera, J. Manrique, Measurement of Stark broadening parameters of FeII and NiII spectral lines by laser induced breakdown spectroscopy using fused glass samples, J. Quant. Spectr. Radiat. Transf 134 (2014) 39–45.
[25] S. Bukvić, A. Srećković, S. Djeniže, Mg II h and k lines Stark parameters, N. Astron. 9 (2004) 629–633.
[26] S. Djeniže, S. Bukvić, A. Srećković, M. Platiša, Mg II spectral line broadening in helium, oxygen and argon-helium plasmas, Astron. & Astrophys 424 (2004) 561–564.
[27] S. Djeniže, S. Bukvić, A. Srećković, Z. Nikolić, The first measured Mn II and Mn III Stark broadening parameters, N. Astron. 11 (2006) 256–261.
[28] R. Mayo, M. Ortiz, Experimental Stark widths of six UV lines of Zn II, J. Phys. B: At. Mol. Opt. Phys. 41 (2008), 225702 (6pp).
[29] J.A. Aguilera, C. Aragón, Characterization of a laser-induced plasma by spatially resolved spectroscopy of neutral atom and ion emissions. Comparison of local and spatially integrated measurements, Spectrochim. Acta, Part B 59 (2004) 1861–1876.
[30] C. Aragón, J.A. Aguilera, Determination of the local electron number density in laser-induced plasmas by Stark-broadened profiles of spectral lines.

Comparative results from Hα, Fe I and Si II lines, Spectrochim. Acta, Part B 65 (2010) 395–400.
[31] S. Zivkovic, J. Savovic, M. Trtica, J. Mutic, M. Momcilovic, Elemental analysis of aluminum alloys by Laser Induced Breakdown Spectroscopy based on TEA CO_2 laser, J. Alloy. Comp. 700 (2017) 175–184.
[32] K.K. Herrera, E. Tognoni, I.B. Gornushkin, N. Omenetto, B.W. Smith, J.D. Winefordner, Comparative study of two standard-free approaches in laser-induced breakdown spectroscopy as applied to the quantitative analysis of aluminum alloy standards under vacuum conditions, J. Anal. At. Spectrom. 24 (2009) 426–438.